HHS Public Access

Author manuscript

Science. Author manuscript; available in PMC 2020 June 23.

Published in final edited form as:

Science. 2019 November 01; 366(6465): 628–631. doi:10.1126/science.aax5440.

Coupled electrophysiological, hemodynamic, and cerebrospinal fluid oscillations in human sleep

Nina E. Fultz[1,2], **Giorgio Bonmassar**[2,3], **Kawin Setsompop**[2,3], **Robert A. Stickgold**[4,5], **Bruce R. Rosen**[2,3], **Jonathan R. Polimeni**[2,3], **Laura D. Lewis**[1,2,*]

[1]Department of Biomedical Engineering, Boston University, Boston, MA 02215, USA.

[2]Athinoula A. Martinos Center for Biomedical Imaging, Massachusetts General Hospital, Boston MA 02129, USA.

[3]Department of Radiology, Harvard Medical School, Boston, MA 02115, USA.

[4]Department of Psychiatry, Beth Israel Deaconess Medical Center, Boston MA 02215.

[5]Department of Psychiatry, Harvard Medical School, Boston, MA 02115, USA.

Abstract

Sleep is essential for both cognition and maintenance of healthy brain function. Slow waves in neural activity contribute to memory consolidation, while cerebrospinal fluid (CSF) clears metabolic waste products from the brain. Whether these two processes are related is not known. We used accelerated neuroimaging to measure physiological and neural dynamics in the human brain. We discovered a coherent pattern of oscillating electrophysiological, hemodynamic, and CSF dynamics that appears during non-rapid eye movement sleep. Neural slow waves are followed by hemodynamic oscillations, which in turn are coupled to CSF flow. These results demonstrate that the sleeping brain exhibits waves of CSF flow on a macroscopic scale, and these CSF dynamics are interlinked with neural and hemodynamic rhythms.

One sentence summary:

During sleep, slow oscillating neural activity precedes coupled waves of blood and cerebrospinal fluid flow in the brain.

Sleep is crucial for both high-level cognitive processing and also basic maintenance and restoration of physiological function. During human non-rapid eye movement (NREM) sleep, the electroencephalogram (EEG) exhibits low-frequency (<4 Hz) oscillatory dynamics that support memory and neural computation (1-8). In addition, functional magnetic resonance imaging (fMRI) studies measuring blood-oxygenation-level-dependent (BOLD) signals have demonstrated widespread hemodynamic alterations during NREM sleep (9-15).

*Correspondence to: ldlewis@bu.edu.

Author contributions: All authors contributed to design; L.D.L. and N.F. collected and analyzed data; L.D.L. wrote the manuscript; all authors edited the manuscript.

Competing interests: L.D.L., B.R.R., and J.R.P. are inventors on a patent coversheet.

Data availability: The ROI and EEG timeseries reported here will be uploaded upon acceptance to Figshare.

Sleep is also associated with increased interstitial fluid volume and clearance of metabolic waste products into the CSF (16), and clearance is stronger in sleep with more low-frequency EEG oscillations (17). Why these diverse physiological processes co-occur within this state of low arousal is not known. In particular, it remains unclear how CSF dynamics change during sleep, and how they relate to the major changes in neural activity and hemodynamics.

We simultaneously measured BOLD fMRI dynamics, EEG, and CSF flow during human sleep. To achieve high temporal resolution imaging, we acquired fMRI data at fast rates (TR<400 ms). While fMRI is often used to detect local oxygenation changes, fast acquisition paradigms also enable detection of fluid inflow: fresh fluid arriving at the edge of the imaging volume has high signal intensity, because it has not yet experienced radiofrequency pulses (Fig. S1). By placing the boundary edge of the imaging volume at the fourth ventricle (Fig. 1a), CSF flow into the brain was detected as increased signal in the lower slices (Fig. 1b), allowing us to measure dynamics of CSF flow simultaneously with BOLD fMRI. We combined this imaging with simultaneous EEG (n=13 subjects) and identified continuous segments of clear stable wake or NREM sleep with low motion (Fig. S2, see Methods), to enable analysis of continuous low-frequency dynamics.

We first asked whether sleep was associated with distinct CSF flow dynamics (Fig. 1c-e). During wakefulness, the CSF signal exhibited a small-amplitude rhythm synchronized to the respiratory signal at ~0.25 Hz (Fig. 1e,g), consistent with previous studies (18, 19). In contrast, during NREM sleep we observed a large oscillation in the CSF signal at 0.05 Hz (Fig. 1e,g). We analyzed this CSF signal across all sleep segments, confirming that identified sleep segments exhibited low-frequency EEG signatures of NREM sleep (Fig. 1f). We found a 5.52 dB increase in the CSF signal peaking at 0.05 Hz during sleep (Fig. 1g,h, Fig. S2; 95% confidence interval (CI)=[2.33 7.67]; p=0.003, signed-rank test), suggesting that large waves of CSF inflow occur approximately every ~20 s. We additionally analyzed nearby non-CSF regions-of-interest (ROIs) with matched slice positioning and saw no such effect (change=−0.03 dB, CI=[−2.7 1.3]; p=0.003 for difference, signed-rank test), suggesting this sleep-associated pattern was specifically driven by physiological signals in the ventricle (Fig. 1i).

Because inflow signals are caused by fluid flowing into the acquisition volume, CSF flow signals should be brightest in edge slices, and decay as fluid passes into central slices (Fig. 2a,b, Fig. S1). We indeed observed a gradient of signal amplitudes across the slices (Fig. 2c,d). Some large inflow events exhibited equally bright amplitudes across the lower slices (Fig. 2d), suggesting the CSF flow velocity had exceeded the imaging critical velocity (11.4 mm/s for slice 2). Together, these results identified large-amplitude pulsatile flow of CSF at 0.05 Hz that appears during NREM sleep.

We next asked whether these slow macroscopic CSF oscillations were linked to hemodynamic signals. Previous studies have proposed microscopic arterial pulsation, corresponding to the ~1 Hz cardiac cycle, as a mechanism for driving interstitial fluid flow (20-23). To test what might generate the much slower macroscopic CSF rhythm we observed, we analyzed the changes in BOLD signal during sleep. We observed an increase

in BOLD signal amplitude in the cortical gray matter fMRI signal during sleep, as compared to wakefulness (Fig. 3a vs. b,c; mean=3.28 dB; CI=[0.09 6.54]; p=0.032, signed-rank test) consistent with previous reports of low-frequency BOLD fluctuations during sleep (9, 10, 24). Furthermore, the CSF signal was tightly temporally coupled to the cortical gray matter BOLD oscillation during sleep (Fig. 3a,b), exhibiting a strong anticorrelation (Fig. S3, max R=−0.48 at lag=2s, p<0.001, shuffling).

This anticorrelation suggested a possible alternation of blood flow and CSF flow during sleep. We hypothesized that the BOLD oscillations corresponded to an oscillation in cerebral blood volume, and that due to constant intracranial volume, more CSF flows into the head when less volume is occupied by the blood (25, 26). This hypothesis predicts that the CSF signal should approximately match the negative derivative of the BOLD oscillation, after setting negative values to zero (see Methods). Consistent with this hypothesis, the CSF timeseries and the thresholded derivative BOLD were strongly correlated (Fig. 3d,e; max R=0.59 at lag −1.8 s; p<0.001, shuffling).

We next examined whether neural activity was linked to these coupled hemodynamic and CSF oscillations during sleep. In conventional fMRI, the BOLD response is elicited by neural activity, which drives flow of oxygen-rich blood (27, 28), and EEG oscillations are associated with hemodynamic signals (29-32). We therefore hypothesized that the large, slow-delta (0.2–4 Hz) electrophysiologic oscillations characteristic of NREM sleep could be coupled to oscillations in blood volume, and in turn displacement effects on CSF flow. We analyzed the instantaneous amplitude of slow-delta EEG relative to the peak of the CSF waves, and found that neural, BOLD, and CSF waves were coupled (Fig. 4a-c; Fig. S4). The neural waves preceded the CSF waves, with a peak in slow-delta EEG occurring 6.4 s prior to the CSF peak (peak amplitude=21%, p<0.001, shuffling). We calculated the best-fit impulse response between the EEG and CSF (Fig. 4d), and found that convolving the EEG with this impulse response yielded significant prediction of CSF dynamics (zero-lag R=0.23, Fig. S5a, cross-validated R=0.22±0.07). To examine whether this EEG-CSF coupling was specifically linked to the appearance of CSF waves during sleep, we tested how well the EEG predicted CSF dynamics in the segments with the largest CSF waves. Performance was higher in segments with larger CSF waves (zero-lag R=0.54, Fig. S5b,c, p<0.001, shuffling), suggesting that the EEG was more strongly linked to CSF in the sleep segments richest in CSF waves.

The coherent dynamics of the EEG, BOLD, and CSF signals thus exhibited a specific timing sequence, with neural rhythms preceding subsequent BOLD and CSF waves. To test whether these observed correlations and delay patterns could arise from biophysical mechanisms, we constructed a computational model using established models of hemodynamic coupling (Fig. 4e, Fig. S6). We extracted the envelope of slow-delta EEG, expected to correlate with decreases in CBF signal due to its associated suppression of neural activity (2). The neural oscillation was then used to predict the timecourses of blood flow, blood volume, and CSF (33, 34). The model first used previously reported physiological parameters (35) with no additional parameter fitting, to test whether our observations were consistent with established biophysical coupling between these signals. This model performed as well as the best-fit impulse response (zero-lag R=0.22; CI across segments=[0.16 0.27]; p<0.001,

shuffling; Fig. S6, S7). The model prediction was significantly larger than the maximal correlation between the original EEG envelope and CSF across all lags (max R=0.15, p<0.05), demonstrating that our data were consistent with biophysical coupling between neural activity, hemodynamics, and CSF.

We conclude that human sleep is associated with large coupled low-frequency oscillations in neuronal activity, blood oxygenation, and CSF flow. While electrophysiological slow waves are known to play important roles in cognition (1), our results suggest that they may also be linked to the physiologically restorative effects of sleep, as slow neural activity is followed by brainwide pulsations in blood volume and CSF flow.

These results address a key missing link in the neurophysiology of sleep. The macroscopic changes in CSF flow we identified are expected to alter waste clearance, as pulsatile fluid dynamics can increase mixing and diffusion (20, 21, 36). Neurovascular coupling has been proposed to contribute to clearance (37), but why it would cause higher clearance rates during sleep was not known. Our study suggests slow neural and hemodynamic oscillations as a new possible contributor to this process, in concert with other physiological factors. Studies in animals could next test for causal relationships between these neural and physiological rhythms.

Our identification of sleep-associated CSF fluid dynamics also suggests a new biomarker to be explored in clinical conditions associated with sleep disturbance. Memory impairment in aging is associated with suppressed slow waves (38); our model suggests this slow wave loss would in turn be associated with decreased CSF flow. Furthermore, our results hint at a potential bridge between recent findings that tau CSF levels and amyloid beta depend on sleep and neural activity (39-41) and that oscillatory neural activity leads to reduced tau (42) — coherent neural activity might signal higher protein aggregate clearance. Taken together, our results identify waves of CSF flow that appear during sleep, and show that slow rhythms in neural activity are interlinked with these CSF waves, with hemodynamic oscillations as an intermediate mechanism through which the two processes are coupled.

Supplementary Material

Refer to Web version on PubMed Central for supplementary material.

Acknowledgments:

We are grateful to Dr. Thomas Witzel for contributing to the imaging, Dr. Jakob Voigts and Dr. Caroline Robertson for comments, and Stephanie Williams, Kanupriya Gupta, and Molly Albrecht for assistance.

Funding: National Institutes of Health R00-MH111748, R01-EB019437, P41-EB015896, R01-MH111419, R01-MH048832, R01-EB024343, R01-MH111438, R21-NS106706, S10-RR023043, S10-OD010759, and the Martinos Center for Biomedical Imaging.

References:

1. Diekelmann S, Born J, Nat Rev Neurosci. 11, 114–126 (2010). [PubMed: 20046194]
2. Steriade M, Nunez A, Amzica F, J Neurosci. 13, 3252–3265 (1993). [PubMed: 8340806]

3. Massimini M, Huber R, Ferrarelli F, Hill S, Tononi G, J Neurosci. 24, 6862–6870 (2004). [PubMed: 15295020]
4. Marshall L, Helgadóttir H, Mölle M, Born J, Nature. 444, 610–613 (2006). [PubMed: 17086200]
5. Destexhe A, Contreras D, in Sleep and Anesthesia, Hutt A, Ed. (Springer Science+Business Media, 2011), p. 258.
6. Van Someren EJW, Van Der Werf YD, Roelfsema PR, Mansvelder HD, da Silva FHL, Progress in Brain Research. 193, 3–15 (2011). [PubMed: 21854952]
7. Vyazovskiy VV, Harris KD, Nat Rev Neurosci. 14, 443–451 (2013). [PubMed: 23635871]
8. Watson BO, Levenstein D, Greene JP, Gelinas JN, Buzsáki G, Neuron. 90, 839–852 (2016). [PubMed: 27133462]
9. Fukunaga M et al., Magnetic Resonance Imaging. 24, 979–992 (2006). [PubMed: 16997067]
10. Horovitz SG et al., Human brain mapping. 29, 671–682 (2008). [PubMed: 17598166]
11. Mitra A, Snyder AZ, Tagliazucchi E, Laufs H, Raichle ME, eLife. 4 (2015), doi:10.7554/eLife.10781.
12. Boly M et al., Proc Natl Acad Sci USA. 109, 5856–5861 (2012). [PubMed: 22451917]
13. Dang-Vu TT et al., Proc Natl Acad Sci USA. 105, 15160–15165 (2008). [PubMed: 18815373]
14. Kaufmann C et al., Brain. 129, 655–667 (2006). [PubMed: 16339798]
15. Larson-Prior LJ et al., Proc Natl Acad Sci USA. 106, 4489–4494 (2009). [PubMed: 19255447]
16. Xie L et al., Science. 342, 373–377 (2013). [PubMed: 24136970]
17. Hablitz LM et al., Sci Adv. 5, eaav5447 (2019). [PubMed: 30820460]
18. Dreha-Kulaczewski S et al., J Neurosci. 35, 2485–2491 (2015). [PubMed: 25673843]
19. Kiviniemi V et al., J. Cereb. Blood Flow Metab. 36, 1033–1045 (2016). [PubMed: 26690495]
20. Schley D, Carare-Nnadi R, Please CP, Perry VH, Weller RO, J. Theor. Biol 238, 962–974 (2006). [PubMed: 16112683]
21. Iliff JJ et al., J Neurosci. 33, 18190–18199 (2013). [PubMed: 24227727]
22. Mestre H et al., Nature Communications, 1–9 (2018).
23. Harrison IF et al., eLife. 7 (2018), doi:10.7554/eLife.34028.
24. Özbay PS et al., Neuroimage. 176, 541–549 (2018). [PubMed: 29704614]
25. Scouten A, Constable RT, Magn. Reson. Med 59, 308–315 (2008). [PubMed: 18228581]
26. Piechnik SK, Evans J, Bary LH, Wise RG, Jezzard P, Magn. Reson. Med 61, 579–586 (2009). [PubMed: 19132756]
27. Ogawa S, Lee TM, Kay AR, Tank DW, Proc Natl Acad Sci. 87, 9868–9872 (1990). [PubMed: 2124706]
28. Kwong KK et al., Proc Natl Acad Sci. 89, 5675–5679 (1992). [PubMed: 1608978]
29. Logothetis NK, Pauls J, Augath M, Trinath T, Oeltermann A, Nature. 412, 150–157 (2001). [PubMed: 11449264]
30. He BJ, Raichle ME, Trends Cogn Sci (Regul Ed). 13, 302–309 (2009). [PubMed: 19535283]
31. Mateo C, Knutsen PM, Tsai PS, Shih AY, Kleinfeld D, Neuron, 1–17 (2017).
32. Schölvinck ML, Maier A, Ye FQ, Duyn JH, Leopold DA, Proc Natl Acad Sci USA. 107, 10238–10243 (2010). [PubMed: 20439733]
33. Buxton RB, Uludağ K, Dubowitz DJ, Liu TT, Neuroimage. 23, S220–S233 (2004). [PubMed: 15501093]
34. Friston KJ, Mechelli A, Turner R, Price CJ, Neuroimage. 12, 466–477 (2000). [PubMed: 10988040]
35. Simon AB, Buxton RB, Neuroimage. 116, 158–167 (2015). [PubMed: 25862267]
36. Asgari M, de Zélicourt D, Kurtcuoglu V, Scientific Reports. 6, 38635 (2016). [PubMed: 27929105]
37. Diem AK, Carare RO, Weller RO, Bressloff NW, PLoS ONE. 13, e0205276 (2018). [PubMed: 30286191]
38. Mander BA et al., Nature Neuroscience. 16, 357–364 (2013). [PubMed: 23354332]
39. Holth JK et al., Science. 363, 880–884 (2019). [PubMed: 30679382]
40. Shokri-Kojori E et al., Proc Natl Acad Sci USA. 115, 4483–4488 (2018). [PubMed: 29632177]

41. Kang J-E et al., Science. 326, 1005–1007 (2009). [PubMed: 19779148]
42. Iaccarino HF et al., Nature. 540, 230–235 (2016). [PubMed: 27929004]
43. Prerau MJ et al., PLoS Comput Biol. 10, e1003866 (2014). [PubMed: 25275376]
44. Luo Q, Huang X, Glover GH, Journal of Neuroscience Methods. 233, 137–149 (2014). [PubMed: 24960423]
45. van der Kouwe AJW, Benner T, Salat DH, Fischl B, Neuroimage. 40, 559–569 (2008). [PubMed: 18242102]
46. Setsompop K et al., Magn. Reson. Med. 67, 1210–1224 (2012). [PubMed: 21858868]
47. Allen PJ, Josephs O, Turner R, Neuroimage. 12, 230–239 (2000). [PubMed: 10913328]
48. Chowdhury MEH, Mullinger KJ, Glover P, Bowtell R, Neuroimage. 84, 307–319 (2014). [PubMed: 23994127]
49. Glover GH, Li TQ, Ress D, Magn. Reson. Med. 44, 162–167 (2000). [PubMed: 10893535]
50. Iber C, Ancoli-Israel S, Chesson AL, Quan SF, The AASM Manual for the Scoring of Sleep and Associated Events (American Academy of Sleep Medicine, Westchester, Illinois, ed. 1, 2007).
51. Greve DN, Fischl B, Neuroimage. 48, 63–72 (2009). [PubMed: 19573611]
52. Fischl B, Neuroimage. 62, 774–781 (2012). [PubMed: 22248573]
53. Kim S, Parker DL, in Magnetic Resonance Angiography: Principles and Applications, Carr JC, Carroll TJ, Eds. (Springer).
54. Bokil H, Andrews P, Kulkarni JE, Mehta S, Mitra PP, Journal of Neuroscience Methods. 192, 146–151 (2010). [PubMed: 20637804]
55. Gao JH, Miller I, Lai S, Xiong J, Fox PT, Magn. Reson. Med. 36, 314–319 (1996). [PubMed: 8843386]
56. Mandeville JB et al., J Cereb Blood Flow Metab. 19, 679–689 (1999). [PubMed: 10366199]

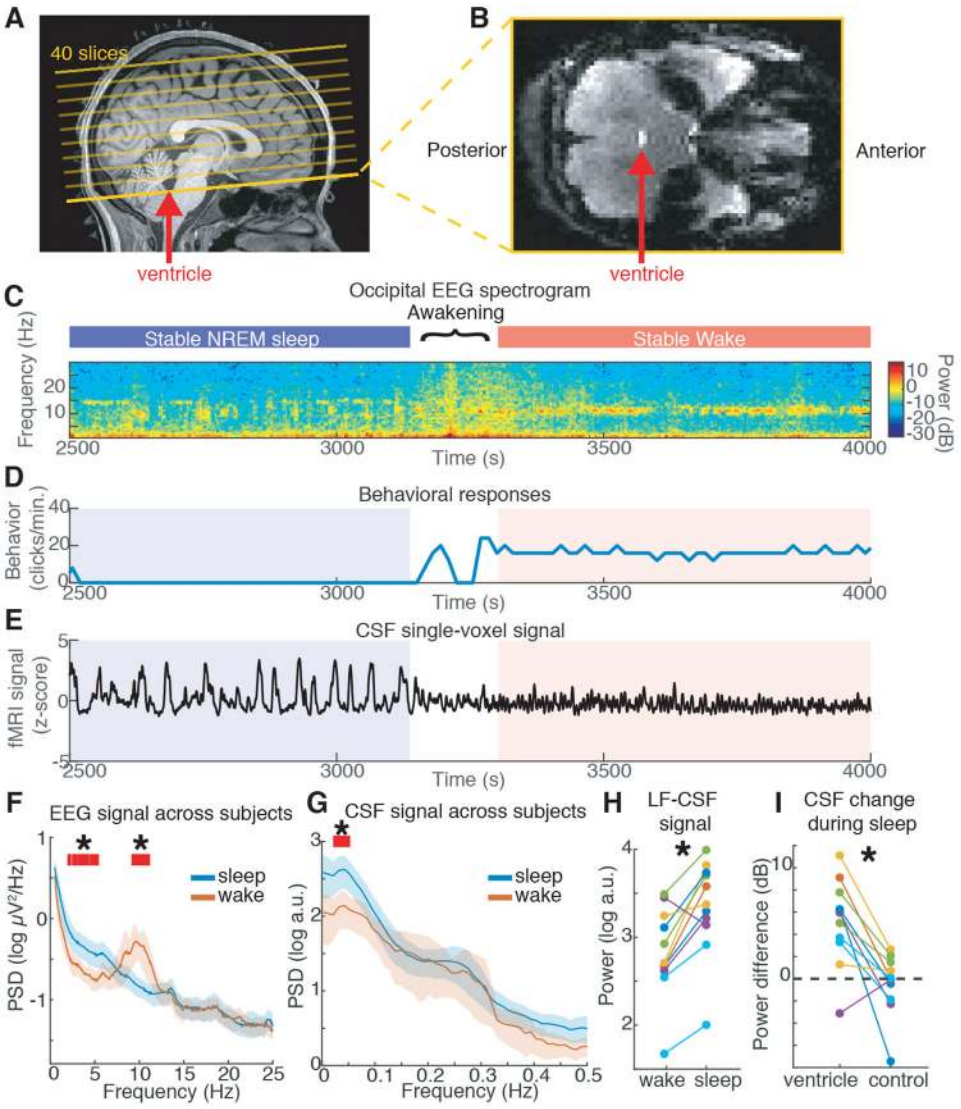

Fig. 1: Large oscillations in CSF signals appear in the fourth ventricle during sleep.

A) Example scan positioning. Thick yellow line: position of the functional image relative to the anatomy. The bottom edge intersects with the fourth ventricle (red arrow), allowing CSF inflow to be measured. A subset of the 40 acquired slices are displayed. B) Example functional image from the bottom slice: inflow through the ventricle is detected as a bright signal (red arrow). C) EEG spectrogram from this subject shows long periods of NREM sleep and wake (~10 Hz occipital alpha). D) Behavioral responses from this subject. E) Timeseries of a single CSF voxel (smoothed with 10-TR kernel) shows large slow dynamics in sleep, that subside during wakefulness. F) Mean power spectral density (PSD) of occipital EEG confirms slow-delta power in sleep, as opposed to high alpha power in wake (n=13 subjects sleep; 11 subjects wake). G) PSD of CSF signal shows increased 0.05 Hz power during sleep (n=13 subjects sleep; 11 subjects wake). Shaded region is 95% CIs; red lines and star mark non-overlapping CIs. H) Low-frequency (LF, 0–0.1 Hz) CSF power increased during sleep (n=11 subjects for pairwise comparison). I) This sleep-selective power increase

was specific to the ventricle ROI and not observed in a neighboring size-matched control ROI (n=11 subjects).

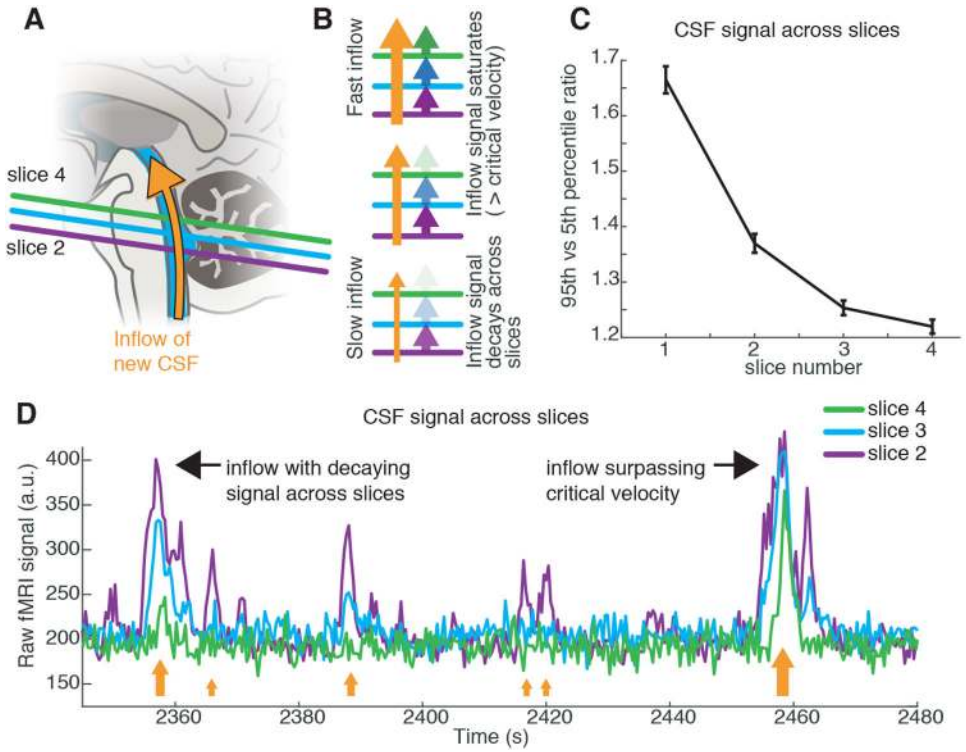

Fig. 2: Ventricle signals correspond to a 0.05 Hz pulsatile inflow of CSF.

A) Schematic of acquisition: new CSF flowing into the imaging volume will generate bright signals. B) Inflow signals will be largest in the bottom slice, and decrease in amplitude inwards. If flow exceeds the critical velocity, then CSF in the bottom slice is completely replaced and signal amplitudes are large in inner slices as well. C) Mean amplitude across slices decays in ascending slices. Error bars are standard error across all sleep segments with the ROI present in 4 contiguous slices (n=129 segments, 11 subjects). D) Example timeseries from the bottom slices of the imaging volume in the 4th ventricle demonstrates largest signal in the lower slices (e.g. 2nd) and smaller signals in higher slices (e.g. 4th). Orange arrows schematically illustrate flow velocity (larger arrows=higher velocity) and black arrows point out individual events.

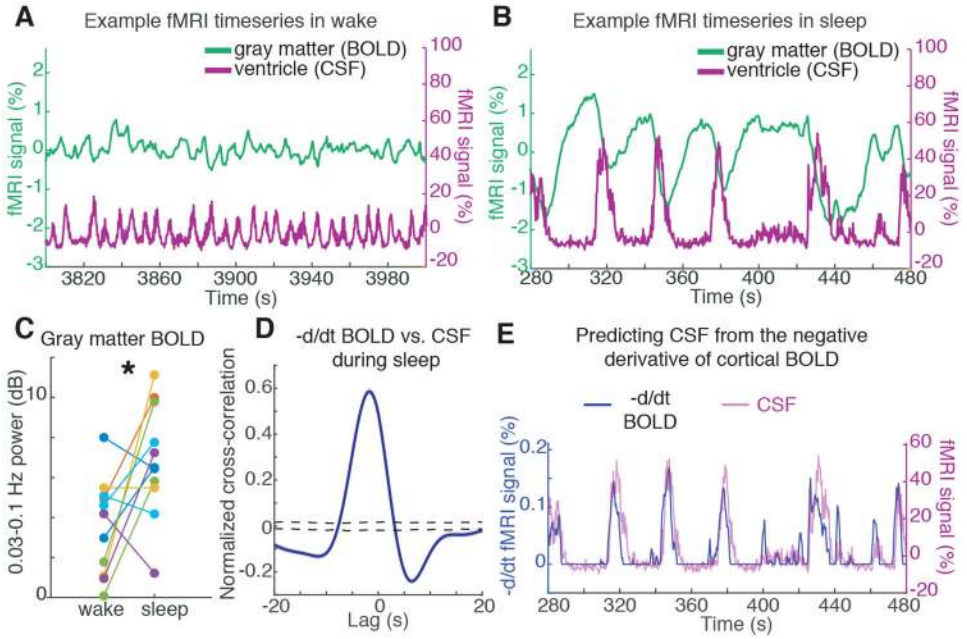

Fig. 3: CSF flow oscillations are anticorrelated to a hemodynamic oscillation in the cortical gray matter that appears during sleep, with CSF flow increasing when blood volume decreases.

A) Example timeseries of the cortical gray matter BOLD signal and the mean CSF signal from one subject. During wake, signals are low-amplitude and synchronized to respiration (0.25 Hz). B) During sleep, a large-amplitude BOLD oscillation appears, and its timecourse is coupled to the ventricle CSF signal (~0.05 Hz). C) The mean cortical gray matter BOLD signal power increases during sleep (n=11 subjects for pairwise test). D) The mean cross-correlation between the zero-thresholded negative derivative of BOLD and CSF signals shows strong correlation (n=176 segments, 13 subjects). Shaded blue is standard error across segments; black dashed line is 95% interval of shuffled distribution. E) Example timeseries showing the correlation, suggesting that CSF flows up the fourth ventricle when cerebral blood volume decreases.

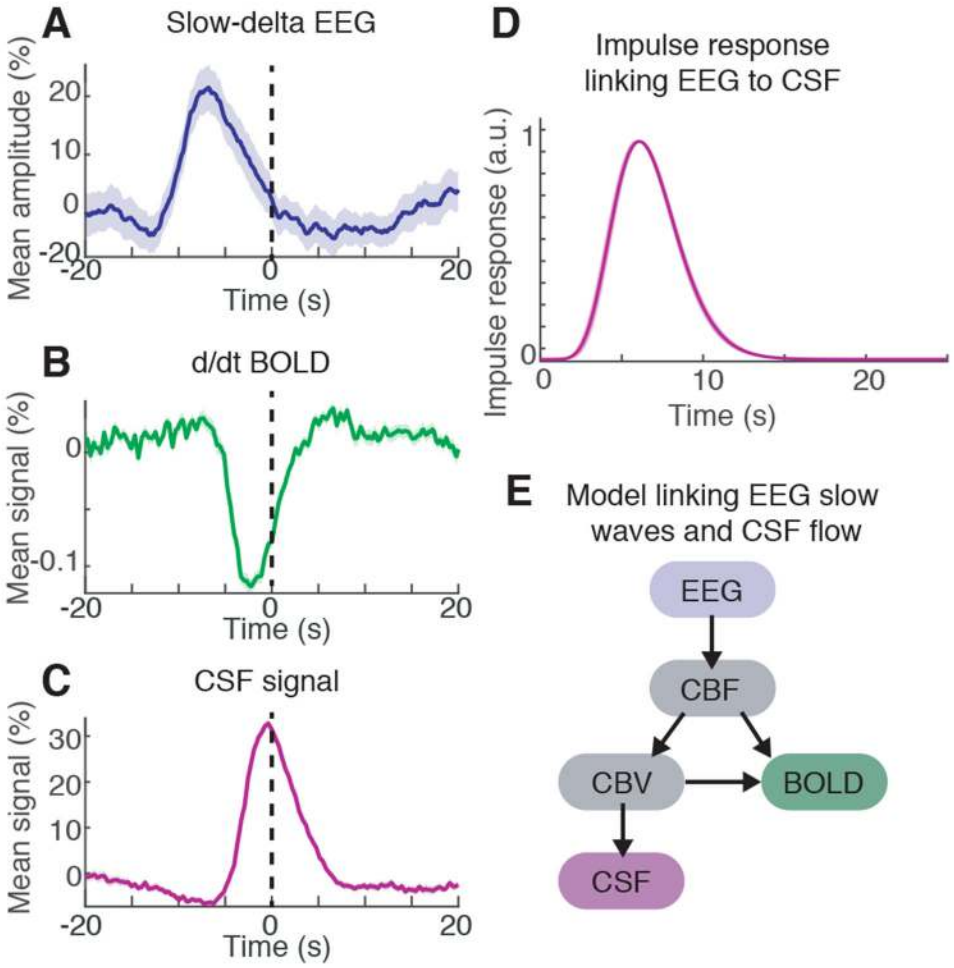

Fig. 4: EEG slow-delta waves are coupled to and precede BOLD and CSF oscillations.

A) The mean amplitude envelope of slow-delta EEG; B) mean derivative of BOLD; and C) mean CSF signal, all locked to the peaks of CSF waves during sleep. Shaded region is standard error across peak-locked trials (n=123 peaks). D) Calculated impulse response of the CSF signal to the EEG envelope shows a similar timecourse to previously established hemodynamic models. Shading is standard deviation across model folds. E) Diagram of model linking the timecourse of neural activity to CSF flow. Variables include cerebral blood flow (CBF) and cerebral blood volume (CBV).